Optimization of a tunable piezoelectric resonator using phononic crystals with periodic electrical boundary conditions

Marie-Fraise Ponge, Bertrand Dubus, Christian Granger, Jerome O. Vasseur, Mai Pham Thi, Anne-Christine Hladky

Available online at www.sciencedirect.com

ScienceDirect

Physics Procedia 70 (2015) 258 – 261

Physics Procedia

2015 International Congress on Ultrasonics, 2015 ICU Metz

Optimization of a Tunable Piezoelectric Resonator Using Phononic Crystals with Periodic Electrical Boundary Conditions

Marie-Fraise Ponge[a], Bertrand Dubus[a], Christian Granger[a], Jérôme Vasseur[b], Mai Pham Thi[c], Anne-Christine Hladky-Hennion[a]

[a]*IEMN UMR 8520 CNRS, dpt ISEN, 41 Boulevard Vauban, 59800 Lille, France.*
[b]*IEMN UMR 8520 CNRS, 59652 Villeneuve d'Ascq, France.*
[c]*Thales Research and Technology, 91120 Palaiseau, France.*

Abstract

Piezoelectric phononic crystals with periodic short-circuit conditions exhibit Bragg band gaps. They are used to design a Fabry-Perot cavity. The design of the device enables a modification of cavity length by a spatial shift of electrical boundary conditions. The resonator is thus tunable and a frequency shift is obtained. An analytical model based on a transfer matrix formalism is used to model longitudinal wave propagation inside the structure. Cavity length, phononic crystal and transducer position are optimized to increase resonance and antiresonance frequency shifts as well as coupling coefficient. Numerical and experimental results are presented and discussed.

Peer-review under responsibility of the Scientific Committee of ICU 2015

Keywords: Phononic crystal; piezoelectric resonator; tunability;

1. Introduction

In communication technology, the development of tunable Surface or Bulk Acoustic Waves resonators to realize adaptable filters is a current technical challenge. Various alternatives have already been investigated [Razafimandimby et al. (2013); Dubus (2013)], but the frequency shift are limited to a few percent and often induces with a change of coupling coefficient or quality fator. Several authors have associated conventional BAW resonators with variable capacitances [Komatsu et al. (2010); El Hassan et al. (2011); Razafimandimby et al. (2013)]. Researchers have also used the intrinsic nonlinear properties of ferroelectric (PZT) [Schreiter et al. (2004); Zinck et al. (2004); Conde et al. (2008)] and paraelectric (BST and STO) [Volatier et. al (2008); Noeth et al. (2010); Vorobiev et al. (2010)] materials.

Phononic crystals [Martinez-Sala et al. (1995); Santos et al. (1987); Kushwaha et al. (1993); Deymier (2013)] are used in RF technology to realize reflective interfaces (Bragg Mirror) [Lakin et al. (2008); Lakin (2004)]. Recently, it has been shown that an homogeneous piezoelectric stack periodically short-circuited presents a Bragg band gap of electrical origin [Degraeve et al. (2014)]. This property is used here to realize a tunable Fabry-Perot cavity.

E-mail address: mariefraise.ponge@gmail.com

Peer-review under responsibility of the Scientific Committee of ICU 2015
doi:10.1016/j.phpro.2015.08.149

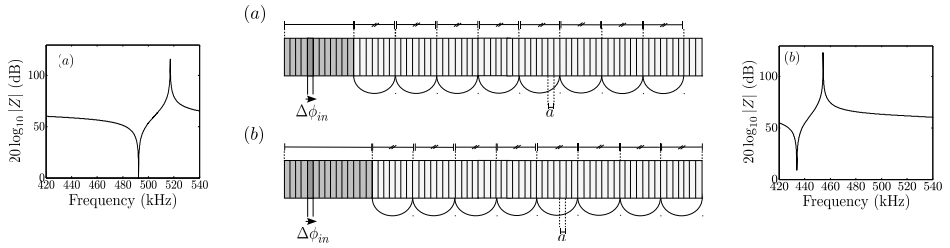

Fig. 1. The Fabry-Perot cavity, in dark grey, is delimited by a PC. The transducer (in darker grey) and cavity (m elements) are at the left edge of the multilayer. The PC is made of piezoelectric elements interconnected every $n = 7$ electrodes. The cavity length L is $12a$ for case (a) and $15a$ for case (b): connections are shifted by $3a$. On (a) (resp. (b)), the transducer is constituted by the fifth element, and resonator impedance is displayed on the left (resp. right) of the figure.

The geometry and physical principles of a tunable Fabry-Perot cavity are first described. The effect of geometrical parameters on the coupling coefficient, series and parallel resonance frequencies are investigated in order to optimize the resonator. Finally, experimental results are presented and discussed.

2. Fabry-Perot Resonator Geometry

Recently, Degraeve *et al.* [Degraeve et al. (2014)] have shown that a stack of short-circuited piezoelectric elements presents band gaps due to the discontinuity of the electric displacement D_3. The band gap frequency range is directly related to the coupling coefficient of the material, the length of short-circuits and the wave velocity. A multilayered structure made of identical piezoelectric elements of length a and section S separated by very thin electrodes is considered. The Fabry-Perot resonator is constituted by a piezoelectric cavity (m elements) stress-free on one side and delimited by a piezoelectric short-circuited phononic crystal on the other side (Fig. 1). One element of the cavity, called "transducer", is electrically driven by an electrical voltage $\Delta\phi_{in}$. Acoustic waves are then generated, they propagate inside the cavity and are reflected on the left by the air/solid interface and on the right by the phononic crystal. The length of the central cavity, and thus its series and parallel resonance frequencies, can be changed by a shift in electrical connections (Figs. 1). The acoustic reflection is maximum when the resonance of the Fabry-Perot cavity is be located inside the band gap of the PC.

3. Modelization of the device

A one-dimensional model, based on an adapted 2*2 transfer matrix formalism, is used to optimize the device [Kutsenko et al. (2015); Ponge et al. (2015)]. Lateral dimension is supposed to be smaller than the cavity and PC lengths. For a stack constituted by a succession of short-circuited elements, considering that the displacements and stresses are continuous at interfaces, the global transfer matrix M of the whole stack is the product of each element transfer matrix. For the Fabry-Perot cavity, the transfer matrices give relationships between displacements and stresses at the boundaries of the device, the cavity, and the transducer. The impedance of the electrical transducer depends on the difference of displacement on both of its sides $U_T^+ - U_T^-$:

$$Z = \frac{\Delta\phi_{in}}{D_3 S} = \frac{\Delta\phi_{in}}{i\omega C_0((U_T^+ - U_T^-)K/C_0 - \Delta\phi_{in})}, \tag{1}$$

with $C_0 = S(1 - k_{33}^2)/(d\beta_{33}^T)$ the clamped capacitance of the element [Wilson (1988)], $K = g_{33}C_0/s_{33}^D$ and $k_{33}^2 = g_{33}^2/(\beta_{33}^T s_{33}^D + g_{33}^2)$. g_{33}, s_{33}^D and β_{33}^T are the electrode area, the piezoelectric constant, the elastic compliance at constant electric displacement and the dielectric impermeability at constant stress, respectively. Assuming that the edges of the stack are stress-free, one can calculate $U_T^+ - U_T^-$ by writing the matrix relations of stresses and displacements between the two edges of the transducer, the cavity and the PC, and by solving the associated system of equations.

The electrical impedance of the resonator is related to its geometry. The length of unit-cells controls the frequency range of the band gap of the piezoelectric PC. The length of the cavity tunes the series and parallel resonance fre-

quencies. For a given vibration mode, when the cavity length increases, series and parallel resonance frequencies decreases ((Fig. 1 (a) and (b))) in the band gap frequency range while coupling coefficient is almost constant. The maximum of the coupling coefficient happens when the transducer coincides with a zone of maximal strain (nodal plane) (Fig. 1 (b))[Ponge et al. (2015); Dubus et al. (2014)]. For a 71 element resonator, an optimal geometry has been found: electrodes are short-circuited every seven electrodes (band-gap: [419-548] kHz) and the fifth element is used as transducer. The tunability of series and parallel resonances is then 27% with an almost constant coupling coefficient of 31%.

4. Experimental results

The prototype (Fig. 2) has been fabricated by the Noliac company. It is composed of a stack of 48 glued PZT (NCE41) disks (diameter 4 mm and thickness 0.5 mm) polarized along the thickness and separated by thin brass electrodes (diameter 4 mm, thickness 40μm). The assembling is realized by gluing piezoelectric elements and electrodes. Electrode strips are welded to flexible electric wires which are welded to a stiffer one arranged on a plugboard.

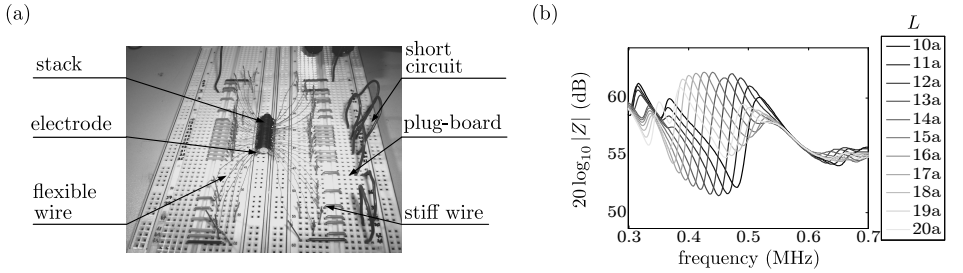

Fig. 2. (a) Experimental set-up: stack of 48 glued PZT (NCE41) disks (diameter 4 mm and thickness 0.5 mm) separated by thin electrodes. Electrodes are arranged alternately and are welded to a flexible electric wire which is welded to a stiffer one arranged on a plugboard. (b) Finite element simulations with 5% damping: the transducer is the fifth of the 48 elements and $10a < L < 20a$.

Additional finite element simulations (ATILA), taking into account a 5% global damping, radial dimension and 48 elements, have been made. They confirm theoretical prediction with a 34% frequency tunability and a 40% coupling coefficient (Fig. 2 (b)).

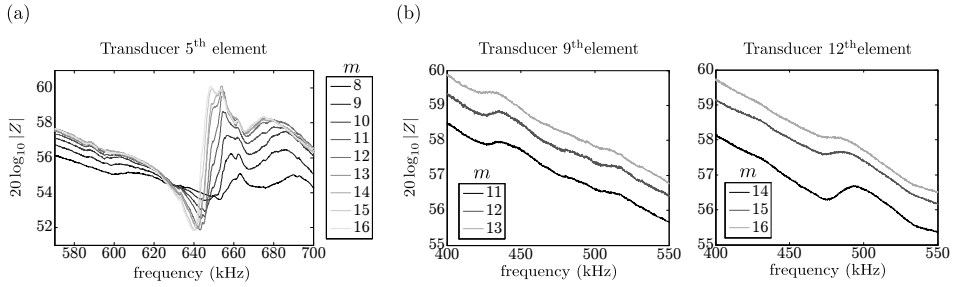

Fig. 3. (a) Experimental impedance versus frequency for a cavity length varying from $L = 8a$ to $L = 16a$ when the transducer is the fifth element. (b) Experimental impedance when the ninth (respectively the twelfth) element is used as the transducer. Cavity length changes from $L = 11a$ (respectively $L = 14a$) to $L = 13a$ (respectively $L = 16a$).

The measured resonance modes shift in the [630-650] kHz frequency range, at higher frequencies than the simulated one and above the theoretical band gap (Fig. 3 (a)). The experimental resonance mode corresponds to a mode of the whole structure modified by electrical conditions [Ponge et al. (2015)]. The tunabilities of series and parallel resonance frequencies and coupling coefficient are presented in Tab. 1. The quality factor of the resonator is low. The measured frequency shift is ten times lower than the predicted value of 30% in the frequency range [419-548]

kHz. This can be explained by the damping, mostly caused by the manufacturing process and the glue layers between NCE41 elements and electrodes.

These conclusions are corroborated by Fig. 3 (b). According to numerical simulations, coupling coefficient should increase when the transducer is moved inside the cavity. Fig. 3 (b) displays electrical impedance when the transducer is situated at the ninth (respectively the twelfth) of the cavity which length changes from $L = 11a$ (respectively $L = 14a$) to $L = 13a$ (respectively $L = 16a$). Additional modes raise in the predicted band gap frequency range [419-548] kHz. They shift slightly to the low frequencies but their amplitude is smaller than the predicted values computed by finite elements simulations (Fig. 2 (b)).

Table 1. Comparison of the frequency shift and coupling coefficient for the 1D model results, FE simulations with 5% of damping and experimental results.

Transducer 5^{th} elements	1D Model	FEM (damping 5%)	Experiments
frequency shift	27%	34%	2.5%
k_{cav}	31%	40%	16%
Cavity lengths	$8a - 16a$	$10a - 20a$	$8a - 16a$
Tuning range (kHz)	419-548	382-505	630-650

5. Conclusion

The optimization of the device results from a compromise between the reflected energy inside the cavity, the electromechanical coupling coefficient and the frequency range of the band gap. It can be obtained by a simple switch of short-circuited electrodes. The results, summarized in Tab. 1, show that difference between simulations and experiment is certainly due to the presence of glue layer between electrodes and piezoelectric elements, and to the complex manufacturing process. Experimental characterization of cavity mode would require a stack with higher quality factor. In the perspective of potential applications, a compromise would be required between a high number of elements, which would lead to a large tunability, and the damping due to the interfaces between piezoelectric elements and electrodes.

References

J. Conde and P. Muralt, *IEEE Trans. Ultrason. Ferroelect. Freq. Contr.*, vol.55(6), pp. 1373–1379, June 2008.
S. Degraeve, C. Granger, B. Dubus, J.O. Vasseur, M. Pham Thi, and A.-C. Hladky-Hennion, *J. of App. Phys.*, vol. 115, pp. 194508, 2014.
P. Deymier, ed, *Acoustic metamaterials and phononic crystals*, Berlin Springer, 2013.
B. Dubus, Future trends in acoustic RF MEMS devices, in *MEMS-based circuits and systems for wireless communication*, C.C. Enz and A. Kaiser, Eds. New York Springer, 2013, pp. 95–117.
B. Dubus, M.-F. Ponge, J.O. Vasseur, M. Pham Thi and A.-C. Hladky-Hennion, *Proc. IEEE Int. Ultrason. Symp.*, 2014, pp. 154–157.
T. Komatsu, K.-Y. Hashimoto, T. Omori and M. Yamaguchi, *Jpn. J. Appl. Phys*, vol. 49(75), 07HD24, July 2010.
M.S. Kushwaha, P. Halevi, L. Dobrzynski, and B. Djafari-Rouhani, *Phys. Rev. Lett.*, vol 71(9), pp. 2022-2025, 1993.
A. A. Kutsenko, A. L. Shuvalov, O. Poncelet and A. N. Darinskii, *J. Acoust. Soc. Am.*, vol. 137(2), pp. 606-616, 2015.
M. El Hassan *et al.*, *Int. J. RF and Microwave Computing-Aided Engng.*, vol. 21(5), pp. 496–504, September 2011.
K.M. Lakin, *Proc. IEEE Ultrason. Symp.*, 2002, pp. 901–908.
K.M. Lakin, G.R. Kline and K.T. McCarron, *IEEE Trans. Microwave Theory. Tech.*, vol. 43(12), pp. 2933–2939, December 1995.
R. Martinez-Sala, J. Sancho, J. V. Sanchez, V. Gomez, J. Llinares, and F. Meseguer, *Nature*, vol. 378, pp. 241, 1995.
A. Noeth *et al.*, *IEEE Trans. Ultrason. Ferroelect. Freq. Contr.*, vol. 57(2), pp. 379–385, February 2010.
M.-F. Ponge *et al.*, *Trans. on Ultr., Ferr., and Freq. Control*, accepted for publication 02/21/2015.
S. Razafimandimby, C. Tilhac, A. Cathelin and A. Kaiser, Tunable BAW filters, in *MEMS-based circuits and systems for wireless communication*, C.C. Enz and A. Kaiser, Eds. New York Springer, 2013, pp. 207–231.
P. V. Santos, L. Ley, J. Mebert, and O. Koblinger, *Phys. Rev. B*, vol. 36(9), pp. 4858-4867, 1987.
M. Schreiter, R. Gabl, D. Pitzer, R. Primig and W. Wersing, *J. Euro. Ceram. Soc.*, vol. 24(6), pp. 1589–1592, 2004.
A. Volatier, E. Defaÿ, M. Aïd, A. N'hari, P. Ancey and B. Dubus, *Appl. Phys. Lett.*, vol. 92(3), pp. 032906, 2008.
A. Vorobiev and S. Gevorgian, *Appl. Phys. Lett.*, vol. 96(21), pp. 212904, 2010.
O.B. Wilson, "*Introduction to theory and design of sonar transducers,*" Los altos Peninsula Publishing, 1988.
C. Zinck, E. Defa, A. Volatier, G. Caruyer, D. Pellissier Tanon and L. Figuiére, *Proc. 14th IEEE Int. Symp. Appl. Ferroelectr.*, 2004, pp. 29–32.